Influence of hydrogenation on the vibrational density of states of magnetocaloric LaFe₁₁.₄Si₁.₆H₁.₆

A. Terwey ●,[1] M. E. Gruner ●,[1] W. Keune,[1] J. Landers ●,[1] S. Salamon ●,[1] B. Eggert ●,[1] K. Ollefs ●,[1] V. Brabänder,[2]
I. Radulov ●,[2] K. Skokov ●,[2] T. Faske ●,[2] M. Y. Hu ●,[3] J. Zhao ●,[3] E. E. Alp ●,[3] C. Giacobbe,[4]
O. Gutfleisch ●,[2] and H. Wende ●[1,*]

[1]*Faculty of Physics and Center for Nanointegration Duisburg-Essen (CENIDE), University of Duisburg-Essen, 47057 Duisburg, Germany*
[2]*Materials Science, TU Darmstadt, 64287 Darmstadt, Germany*
[3]*Advanced Photon Source (APS), Argonne National Laboratory, Lemont, Illinois 60439, USA*
[4]*European Synchrotron Radiation Facility (ESRF), 38000 Grenoble, France*

We report on the impact of magnetoelastic coupling on the magnetocaloric properties of LaFe₁₁.₄Si₁.₆H₁.₆ in terms of the vibrational (phonon) density of states (VDOS), which we determined with ^{57}Fe nuclear resonant inelastic x-ray scattering (NRIXS) measurements and with density functional theory (DFT) based first-principles calculations in the ferromagnetic (FM) low-temperature and paramagnetic (PM) high-temperature phase. In experiments and calculations, we observe pronounced differences in the shape of the Fe-partial VDOS between nonhydrogenated and hydrogenated samples. This shows that hydrogen not only shifts the temperature of the first-order phase transition, but also affects the elastic response of the Fe subsystem significantly. In turn, the anomalous redshift of the Fe VDOS, observed by going to the low-volume PM phase, survives hydrogenation. As a consequence, the change in the Fe-specific vibrational entropy ΔS_{lat} across the phase transition has the same sign as the magnetic and electronic contribution. DFT calculations show that the same mechanism, which is a consequence of the itinerant electron metamagnetism associated with the Fe subsystem, is effective in both the hydrogenated and the hydrogen-free compounds. Although reduced by 50% as compared to the hydrogen-free system, the measured change ΔS_{lat} of $(3.2 \pm 1.9) \frac{\text{J}}{\text{kg K}}$ across the FM-to-PM transition contributes with ∼35% significantly and cooperatively to the total isothermal entropy change ΔS_{iso}. Hydrogenation is observed to induce an overall blueshift of the Fe VDOS with respect to the H-free compound; this effect, together with the enhanced Debye temperature observed, is a fingerprint of the hardening of the Fe sublattice by hydrogen incorporation. In addition, the mean Debye velocity of sound of LaFe₁₁.₄Si₁.₆H₁.₆ was determined from the NRIXS and the DFT data.

I. INTRODUCTION

In the search for an environmentally friendly alternative to the conventional gas-compressor refrigeration, solid state cooling concepts offer an energy-efficient perspective [1,2]. First-order magnetocaloric materials are considered as one important class of systems for this purpose [3–7]. Moreover, magnetocaloric materials are considered for local heating and cooling inside the human body [8]. These materials are characterized by a significant adiabatic temperature change $|\Delta T_{\text{ad}}|$ induced by magnetic fields and a large isothermal entropy change $|\Delta S_{\text{iso}}|$ at a magnetostructural phase transition at the phase transition temperature, T_{tr}.

Among the materials of current interest with a large magnetocaloric effect and ability to be tailored to possible user applications are LaFe₁₃₋ₓSiₓ-based compounds [9–15]. Their isostructural first-order phase transition at T_{tr} is accompanied by a drastic volume decrease with narrow hysteresis [16,17], which is associated with an itinerant electron metamagnetic transition (IEM) [1,4,12,13,18–20]. For Si contents of $1.2 \leqslant x \leqslant 2.5$, LaFe₁₃₋ₓSiₓ-based compounds tend to crystallize in

a cubic NaZn₁₃ ($Fm\overline{3}c$) structure (1:13 phase). The prototype structure is usually represented by a 112-atom unit cell with cubic (Cartesian) axes containing two nonequivalent Zn (Fe) sites. Here, we refer with Fe$_{\text{II}}$ to the 96-fold (96i) sites, which exhibit a lower local symmetry, while Fe$_{\text{I}}$ corresponds to the highly symmetrical 8-fold (8b) Wyckoff positions. It is widely assumed that Si occupies the 96i sites randomly, shared with Fe$_{\text{II}}$ [21,22]. The transition temperature in these compounds increases with Si content and turns the phase transition from first to second order, with a reduction in both $|\Delta T_{\text{ad}}|$ and $|\Delta S_{\text{iso}}|$ [23,24]. To avoid this, the incorporation of hydrogen into these compounds leads to the occupation of the interstitial lattice sites (24d) by hydrogen, while retaining a first-order phase transition [22,25,26]. Occupation of all 24d sites by hydrogen corresponds to $y = 3$ H per formula unit. However, in experiment the 24d sites are never fully occupied and the hydrogen content in LaFe₁₃₋ₓSiₓH$_y$ does not exceed a value of $y = 1.8$ depending on the composition [27,28]. This is discussed as a result of the nonbonding or even repulsive character of the Si-H interaction [22,29]. A similar behavior is observed for other hydrogenated compounds than La(FeSi)₁₃H$_y$ containing transition metals and main-group elements [30].

Figure 1 depicts the primitive cell with a fcc base containing 34 atoms and hydrogen on the interstitial (24d) lattice
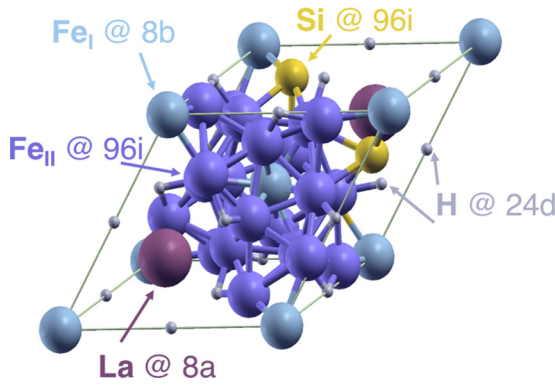
*heiko.wende@uni-due.de

FIG. 1. Primitive cell with fcc base for hydrogenated LaFe$_{11.5}$Si$_{1.5}$H$_3$ consisting of 34 atoms. The color code for the atoms is as follows: La at 8a (brown), Fe$_I$ at 8b (light blue), Fe$_{II}$ at 96i (dark blue), Si at 96i (yellow), and H at 24d (gray).

sites. Interstitial hydrogenation can provide a first-order phase transition while retaining good magnetocaloric performance and maintaining a large adiabatic temperature change $|\Delta T_{ad}|$ and entropy change $|\Delta S_{iso}|$ [31–35]. Hydrogenation and additional incorporation of Mn into these compounds gives the opportunity to specifically tailor the transition to temperatures as needed, covering a broad temperature range (135–345 K) [26] without changing the lattice symmetry [26,36] as H increases and Mn decreases the transition temperature drastically. This makes hydrogenated LaFe$_{13-x}$Si$_x$-based compounds promising materials for room temperature cooling applications.

The total isothermal entropy change ΔS_{iso} is often decomposed into independent contributions from the elemental constituents or the relevant degrees of freedom [18,37,38]:

$$\Delta S_{iso} = \Delta S_{mag} + \Delta S_{lat} + \Delta S_{el}. \tag{1}$$

The terms on the right-hand side refer to the magnetic, lattice (vibrational), and electronic degrees of freedom, respectively. One has to bear in mind that these contributions cannot be separated in a strict sense, since cross-coupling between the different degrees of freedom—such as magnetoelastic or electron-phonon coupling—must be expected [18,39–43]. Nevertheless, the simple decomposition, Eq. (1), still gives a useful indication of the extent to which a particular set of degrees of freedom contributes to the magnetocaloric performance of a material.

In this work we will illustrate the effect of hydrogenation on the lattice dynamics and thermodynamic properties as well as the structure of the vibrational density of states (VDOS) of LaFe$_{13-x}$Si$_x$-based compounds by means of temperature-dependent ^{57}Fe nuclear resonant inelastic x-ray scattering (NRIXS) and density functional theory (DFT) calculations. NRIXS is directly sensitive to the Fe-specific lattice dynamics only [44–47], while DFT provides access to the contributions from all elements. The measurement of the phonon excitation probability provides direct access to the ^{57}Fe-partial VDOS $g(E)$ and the vibrational entropy S_{lat}.

In our present work, we tackle the following open fundamental questions for hydrogenated magnetocaloric La(FeSi)$_{13}$H compounds: (i) What is the impact of interstitial hydrogen atoms on the vibrational (phonon) density of states,

the latter being a basic property for the understanding of vibrational thermodynamics, such as the vibrational (lattice) entropy ΔS_{lat}? (ii) How does the hydrogenation affect the jump of ΔS_{lat} in the temperature dependence of the vibrational entropy observed previously at the FM-to-PM transition in the nonhydrogenated parent material [39,42]? As suggested earlier [43], corresponding investigations may provide a significant contribution to quantify the role of electron coupling to the lattice degrees of freedom as a function of hydrogenation. (iii) Is the magnetostructural first-order FM-to-PM phase transition in the hydrogenated material reflected in the T dependence of the average velocity of sound, $\langle v_D \rangle$, as determined from the NRIXS data? In the literature, this method has been applied to the magnetocaloric (Mn, Fe)$_{1.95}$(P, Si) compound, and $\langle v_D \rangle$ was shown to be larger in the FM state than in the PM state [48].

II. METHODS

Experiments have been performed on polycrystalline powder samples (particle size $\leqslant 100\,\mu$m) with a nominal composition of LaFe$_{11.4}$Si$_{1.6}$H$_y$ and $y \approx 1.6$. For better data quality in the NRIXS measurements, the samples are enriched to 30% in the ^{57}Fe isotope. The samples were prepared at the TU Darmstadt by arc melting in Ar atmosphere and subsequent annealing at 1373 K for 7 days in an Ar-filled quartz tube followed by quenching in water. The hydrogenation was done by heating the sample in a furnace at 0.9 bar H$_2$ atmosphere at 723 K for one hour according to the procedures described in Refs. [14,26].

For the experiments, the ingots were crushed and ground into a powder, as in our former work [39,42]. High-resolution powder x-ray diffraction (HR-PXRD) measurements, performed at beamline ID22 of the ESRF, revealed the 1:13 phase with only α-Fe as a secondary phase (see the Supplemental Material [49]; see also Refs. [50–55] therein). The powder prepared for the experiments leads to two samples, A and B, with slightly different residual secondary-phase contents. Pre-characterization has been performed via temperature-dependent vibrating sample magnetometry using a Quantum Design PPMS DynaCool to determine the transition temperature and thermal hysteresis of the compounds. Magnetization measurements revealed a first-order IEM transition from a ferro- (FM) to paramagnetic (PM) state at $T_{tr} = 329$ K in an applied field of $\mu_0 H = 10$ mT for the hydrogenated compounds (see Fig. S1 of the Supplemental Material [49]). Their thermal hysteresis obtained by magnetometry is narrow, with a width of only 3 K. Field-dependent magnetometry up to 9 T revealed a very good sample quality with a very small α-Fe content (secondary phase) of 1.91% (sample A) and 4.47% (sample B). Furthermore, we have performed temperature-dependent PXRD measurements on an independently prepared hydrogenated LaFe$_{11.4}$Si$_{1.6}$H$_{1.6}$ powder sample of natural isotopic composition (sample C) in order to determine the T dependence of the mass density, ρ, from the lattice parameter. Details are given in the Supplemental Material [49].

To gather information on the lattice dynamics and to obtain the VDOS, ^{57}Fe NRIXS [45–47,56,57] measurements have been performed at Sector 3-ID at the Advanced Photon Source, Argonne National Laboratory. The energy of the

incident x-ray beam was tuned around the nuclear resonance energy of $E_0 = 14.412$ keV of ^{57}Fe. The energetic bandwidth of the x-ray beam is reduced with the use of a high-resolution silicon crystal monochromator to a value of 1 meV [58]. After passing through a toroidal mirror, the collimated beam was focused onto the sample at grazing incidence relative to the flat sample surface. An avalanche photodiode detector with timing electronics [59] was used to detect the 6.4 keV fluorescence x-ray signal emitted only with the delayed nuclear resonant scattering events and the 14.4 keV fluorescence of the nuclear resonance. For the low-temperature data the sample was placed in a closed-cycle cryostat under a dome-shaped Be window. For the data above room temperature the samples were mounted on a custom-built heater at atmospheric pressure. For the NRIXS measurements the powder samples were embedded in epoxy resin on a Cu plate providing a macroscopically flat sample surface. The experiments were performed in zero external magnetic field as well as with an applied field of 1.1 T by permanent magnets. Multiple temperature points were taken across T_{tr} and in the sample's well-defined FM and PM state far away from T_{tr} to precisely evaluate the changes in the VDOS during the magnetostructural phase transition. For temperature control a LakeShore 340 temperature controller with PID regulation was used with either a silicon diode temperature sensor or a K-type thermocouple, providing a temperature accuracy of ±0.1 K. The Fe-partial VDOS was extracted from the NRIXS data using the Pi program [60] with correction for residual α-Fe contents mentioned earlier. As the ratio of crystallographic abundance of Fe$_I$ 8b to Fe$_{II}$ 96i sites in the La(Fe, Si)$_{13}$ compound is 1:12, the measured Fe VDOS is typical for the dominant Fe$_{II}$ species.

In our parameter-free first-principles calculations, we added 3 H ions to the 24d positions of the 28-atom primitive cell of the hydrogen-free compound described earlier [39,61], which has three Si atoms placed on the 96i sites of Fe. The cell thus corresponds to two formula units (f.u.) of LaFe$_{11.5}$Si$_{1.5}$H$_{1.5}$ which is a good approximation of the sample stoichiometry used in the experiments. According to Rosca *et al.* [22], we selected only those sites that do not have Si atoms on neighboring 96i positions, which is one half of the 6 available 24d sites in the primitive cell. Indeed, our calculations show that this configuration is lower in energy by 316 meV/H in comparison with the exclusive occupation of the remaining sites, which do have Si in their nearest neighborhood. The calculations were carried out with the Vienna *Ab initio* Simulation Package (VASP) [62,63]. The setup is similar to that for the hydrogen-free case (see Refs. [39,61] for further details). Exchange and correlation was described with the PW91 functional of Perdew and Wang [64,65] in combination with the spin interpolation formula of Vosko, Wilk, and Nusair [66] and a cutoff energy of $E_{cut} = 380$ eV. Structural optimizations were carried out on a k mesh of a $9\times9\times9$ grid, which yields 125 k points in the irreducible Brillouin zone (IBZ), while for the electronic density of states (DOS) we used a $15\times15\times15$ k grid. For the final presentation, the DOS was convoluted with a Gaussian ($\sigma = 0.1$ eV). The calculation of the VDOS is based on the so-called direct or force-constant approach [67–69]. It was calculated with the PHON code by Alfè [70] using the forces obtained with

VASP from 62 individual displacements of 0.02 Å of the inequivalent ions in a $2\times2\times2$ (248 atom) supercell. The PM state was represented by a static pseudo-disordered, nearly antiferromagnetic spin configuration, as for the hydrogen-free case [39,61], which was stabilized by a fixed-spin-moment constraint [71–74] to retain a residual magnetic moment of 3.75 μ_B/f.u., similarly to Ref. [39].

III. RESULTS AND DISCUSSION

A. NRIXS and VDOS

The top graph in Fig. 2 shows the (partial) Fe VDOS of nonhydrogenated undoped and hydrogenated LaFe$_{13-x}$Si$_x$
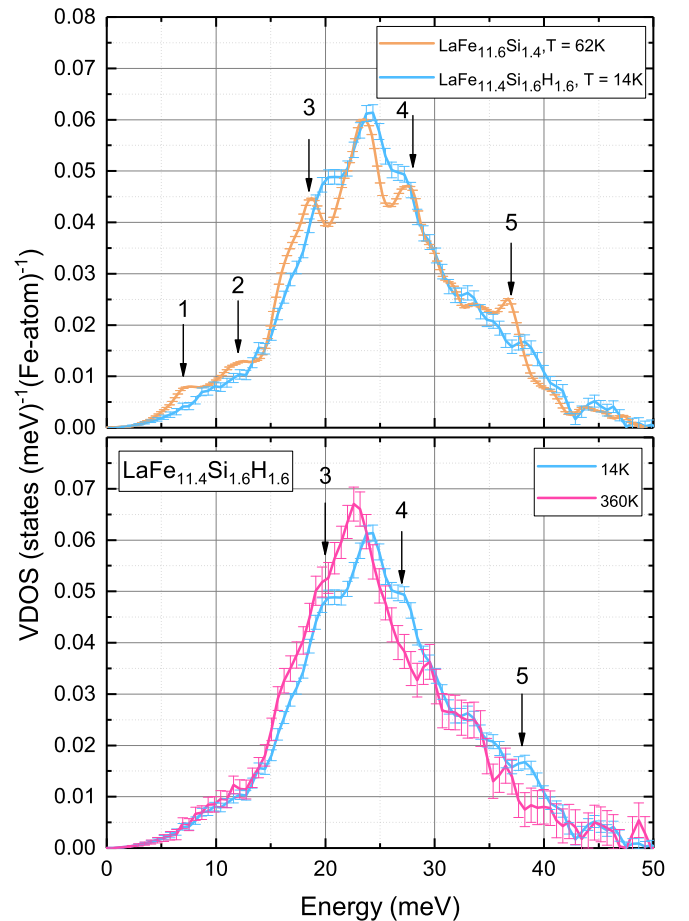

FIG. 2. Top: Comparison of the Fe-partial VDOS of LaFe$_{11.6}$Si$_{1.4}$ (reference sample, orange line) and hydrogenated LaFe$_{11.4}$Si$_{1.6}$H$_{1.6}$ (blue line). The VDOS were derived from corresponding NRIXS spectra taken at low temperatures, i.e., at 62 K for LaFe$_{11.6}$Si$_{1.4}$ (data taken from [39]) and at 14 K for LaFe$_{11.4}$Si$_{1.6}$H$_{1.6}$, in the FM phase. The black arrows, labeled 1–5 at phonon energies E of 7, 12, 18, 28, and 36 meV, respectively, depict the energetic positions, where sharp peaks exist for the nonhydrogenated samples, and where remarkable changes in the VDOS after hydrogenation are apparent. Bottom: Comparison of the Fe-partial VDOS of the LaFe$_{11.4}$Si$_{1.6}$H$_{1.6}$ sample in its FM phase at 14 K (blue line) and in its PM phase at 360 K (pink line). The black arrows at energetic values of 20, 27, and 38 meV depict the change in the VDOS, which occurs after undergoing the metamagnetic phase transition at $T_{tr} = 329$ K. All data were measured in zero external field. The VDOS with hydrogenation was obtained from sample A with correction of an α-Fe content of 1.91%.

compounds obtained by ^{57}Fe NRIXS. The LaFe$_{11.6}$Si$_{1.4}$ sample (reference sample) is identical to the specimen studied in [39] and has been selected for comparison with our present hydrogenated sample that is close to the reference sample in Fe and Si content. Representative NRIXS spectra (raw data) and normalized excitation probability spectra are presented in the Supplemental Material [49]. The spectra depicted in Fig. 2 are both taken at low temperature at zero external field in the FM phase, i.e., at $T = 14$ K (LaFe$_{11.4}$Si$_{1.6}$H$_{1.6}$) and $T = 62$ K (LaFe$_{11.6}$Si$_{1.4}$). The low-temperature (partial) VDOS of LaFe$_{11.6}$Si$_{1.4}$ exhibits a dominant peak at $\sim$23.5 meV with weaker peaks 3 and 4 at $\sim$18 and $\sim$28 meV, respectively. Moreover, there are weak low-energy peaks near $\sim$7 meV and $\sim$12 meV, numbered 1 and 2, respectively, and a weak high-energy peak at $\sim$37 meV.

We observe striking differences between the Fe-partial vibrational density of states with (blue line) and without hydrogenation (orange line) for the FM state (Fig. 2, top). In the hydrogenated sample the shape of the VDOS drastically changes with respect to the undoped sample, and the phonon peaks are broadened and shifted. Especially the features at about 7, 12, 18.5, 28, and 37 meV, which are marked by the black arrows, are affected. Peaks 1 and 2 at 7 and 12 meV are reduced to a very low amplitude and are smoothed out by hydrogenation, while peaks 3, 4, and 5 at 18.5 meV, 28 meV, and 37 meV are reduced to broad shoulders and energetically redistributed. We observe an energetic blueshift of peak 3 (near 18 meV), a slight blueshift of the main peak (near 24 meV), a slight redshift for peak 4 (near 27 meV), and a suppression of peak 5 (near 37 meV), all of these modifications being induced by hydrogenation in the FM phase (blueshift: shift to higher phonon energies E; redshift: shift to lower phonon energies).

To see an imprint of the phase transition onto the vibrational density of states, the VDOS in the two magnetic states have been compared. The Fe-partial VDOS in the low-temperature FM phase at $T = 14$ K ($T \ll T_{tr}$, blue line) and in the high-temperature PM phase at $T = 360$ K ($T > T_{tr}$, pink line) of hydrogenated LaFe$_{11.4}$Si$_{1.6}$H$_{1.6}$ in Fig. 2 (bottom) reveal clear differences. It can be seen that the residual phonon peaks (shoulders) in the VDOS of the FM state (black arrows, numbered 3–5) at 20, 27, and 38 meV are modified. Peaks 3 and 5 are nearly completely quenched in the PM state. In particular the phonon mode 4 visible at 27 meV in the FM state is drastically suppressed in the PM state and smoothed out. This is a microscopic signature of strong magnetoelastic (spin-phonon) coupling of the Fe magnetic moments in the FM phase in hydrogenated LaFe$_{11.4}$Si$_{1.6}$H$_{1.6}$, thus exhibiting similar behavior to that observed in our previous studies on nonhydrogenated LaFe$_{13-x}$Si$_x$ [39,42]. The peak reduction in the PM state in the hydrogenated sample is less pronounced than in nonhydrogenated compounds, but the phonon peak at $\sim$27 meV still vanishes as soon as large magnetic disorder is introduced into the sample.

A similar effect occurs for the $\sim$18 meV peak (3), which survives the FM-to-PM transition in the nonhydrogenated material [42], but is strongly suppressed in the PM state of the hydrogenated compound, where it appears as a blueshifted shoulder at $\sim$20 meV (see Fig. 3).

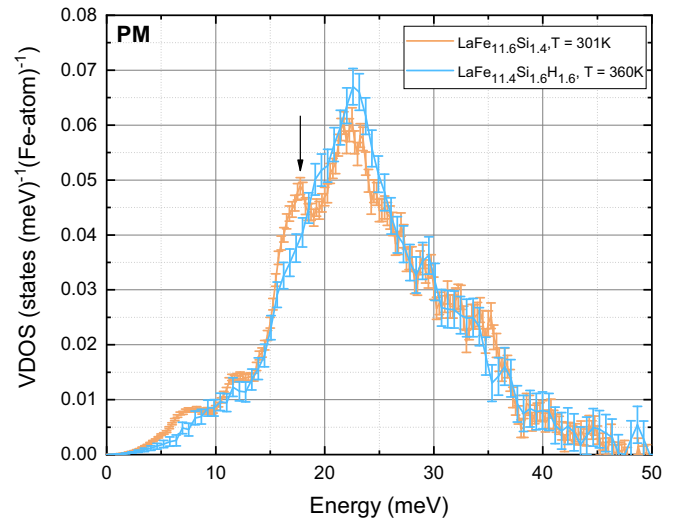FIG. 3. Fe-partial VDOS of LaFe$_{11.6}$Si$_{1.4}$ at 301 K (orange, from Ref. [42]) and LaFe$_{11.4}$Si$_{1.6}$H$_{1.6}$ at 360 K (blue, present work, sample A), both samples being in the PM state. The phonon mode at $\sim$18 meV (marked by the arrow) of the nonhydrogenated compound is strongly suppressed in the H-containing compound. Hydrogenation leads to an overall energetic blueshift of the VDOS in the PM state.

Thus, magnetic disorder occurs upon heating above the phase transition temperature $T_{tr} = 329$ K and the formation of the paramagnetic state, leading to distinct modifications in the VDOS.

Most importantly, comparing the magnetically ordered (FM) and disordered (PM) states, a uniform shift of the phonon modes to lower phonon energies (redshift) is visible in the VDOS of Fig. 2, bottom, which, as will be shown below, yields an overall increase in the vibrational entropy. The total redshift, which can be seen in Fig. 2 (bottom), can be quantified in terms of the first ($n = 1$) moment of the VDOS $g(E)$,

$$\langle E^n \rangle = \int_0^\infty E^n g(E)\, dE, \qquad (2)$$

where we assume the integral over $g(E)$ to be normalized to 1. We would like to emphasize that according to this definition, $\langle E^1 \rangle$ is distinct from the phonon inner energy $U(T)$ as it does not include the Bose-Einstein factor and, therefore, does not include the temperature-dependent phonon occupation probability. $\langle E^1 \rangle$ as a function of temperature for LaFe$_{11.4}$Si$_{1.6}$H$_{1.6}$ and for the reference sample LaFe$_{11.6}$Si$_{1.4}$ is displayed in Fig. S10 of the Supplemental Material [49]. The decrease of $\langle E^1 \rangle$ amounts to an energetic redshift of -3.1% upon heating over the entire measured temperature range from 14 K to 360 K for LaFe$_{11.4}$Si$_{1.6}$H$_{1.6}$, while this redshift is -3.7% in the measured range from 62 K to 301 K for nonhydrogenated LaFe$_{11.6}$Si$_{1.4}$ (see Fig. S10). Interestingly, in the case of the nonhydrogenated reference sample, a sharp drop of $\langle E^1 \rangle$ by -2.6% (redshift) is observed at $T_{tr} = 192$ K upon heating, with an estimated width of the transition of 20 K (see Fig. S10). For LaFe$_{11.4}$Si$_{1.6}$H$_{1.6}$, the drop in $\langle E^1 \rangle$ at $T_{tr} = 329$ K (redshift) is reduced to -1.3%, which is about half of that of the nonhydrogenated compound, while the width of the

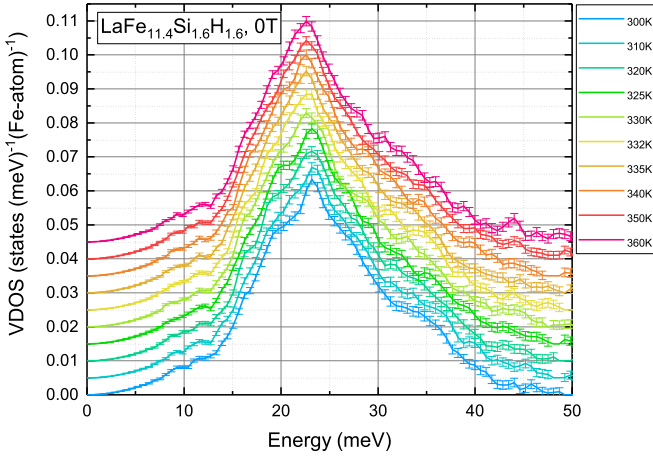FIG. 4. Fe-partial VDOS of $LaFe_{11.4}Si_{1.6}H_{1.6}$ measured across the phase transition in zero applied magnetic field and obtained by NRIXS at different temperature points, measured closely around the metamagnetic phase transition, from 300 K (bottom line, blue) to above the transition at 360 K (top line, pink) following a color gradient ($T_{tr} = 329$ K). The curves are vertically shifted by 0.005 states $(meV)^{-1}$ (Fe atom)$^{-1}$ for better visualization. These VDOS have been corrected for a residual α-Fe content of 4.47% (sample B) and correspond to the entropy points at 0 T of Fig. 5.

transition is much larger ($\sim$50 K) than that of the nonhydrogenated material. This redshift (upon heating at the transition temperature) occurs despite the large volume decrease of $\sim$1%, which contradicts the expected behavior following Grüneisen theory [39,42,75]. From Grüneisen theory, one would expect a blueshift ($\frac{\Delta E}{E} > 0$) in phonon energy E (and not a redshift $\frac{\Delta E}{E} < 0$) according to the Grüneisen relation $\frac{\Delta E}{E} = -\gamma(\frac{\Delta V}{V})$, where $\gamma > 0$ is the average Grüneisen constant, and $\frac{\Delta V}{V} < 0$ the relative atomic volume contraction at the isostructural FM-to-PM transition at T_{tr} for $LaFe_{11.4}Si_{1.6}H_{1.6}$. The redshift implies a lattice softening in the PM phase, which has also been observed in previous studies on nonhydrogenated $LaFe_{13-x}Si_x$ compounds [39,42]. In the low-energy regime ($E < 14$ meV), almost no changes in the shape of the VDOS are visible in Fig. 2 (bottom). This results from the weak intensity of the phonon modes at low energies. Figure 4 shows the VDOS at zero external field of $LaFe_{11.4}Si_{1.6}H_{1.6}$ at six temperature points above and four points below the metamagnetic phase transition region, across T_{tr}. The data correspond to sample B and have been corrected for a residual α-Fe content of 4.47% as in our former work [39,42]. Significant changes in the VDOS appear closely above and closely below $T_{tr} = 329$ K at phonon modes near 20 and 27 meV. These phonon modes decay upon heating across T_{tr} and the whole VDOS shifts to lower energies due to the lattice softening with increasing temperature.

So far we have mostly described the influence of temperature on the VDOS. In the following we will discuss the impact of hydrogenation on the phonon DOS in the low-temperature FM state and in the high-temperature PM state and the respective overall energetic shifts of the VDOS (see Fig. S10 of the Supplemental Material [49]). In the low-temperature FM state (Fig. 2, top) the first moment of the VDOS $\langle E^1 \rangle$ of

TABLE I. Entropy Debye temperatures Θ and sound velocities $\langle v_D \rangle$ associated with the Fe-subsystem and the total VDOS obtained from NRIXS measurements and DFT calculations together with the first moment $\langle E^1 \rangle$ of the Fe-partial VDOS.

	Θ^{Fe} (K)	Θ^{tot} (K)	$\langle v_D^{Fe} \rangle$ (m/s)	$\langle v_D^{tot} \rangle$ (m/s)	$\langle E^1 \rangle$ (meV)
14 K	386 ± 7		3120 ± 45		25.22
300 K	377 ± 1		3030 ± 16		24.65
360 K	373 ± 1		3020 ± 16		24.45
DFT-FM	391	436	3064 ± 69	3002 ± 117	25.60
DFT-PM	369	420	2931 ± 173	2894 ± 159	24.22

nonhydrogenated $LaFe_{11.6}Si_{1.4}$ at 62 K is 24.68 meV, whereas $\langle E \rangle = 25.22$ meV for hydrogenated $LaFe_{11.4}Si_{1.6}H_{1.6}$ at 14 K. We may neglect the tiny overall redshift of about 0.1% expected between 14 K and 62 K upon warming. Then, the influence of hydrogenation on the overall VDOS is a striking energetic blueshift of +2.1% in the low-T FM state, as Fig. S10 demonstrates. Also in the PM state we find an apparent overall blueshift through hydrogenation (see Fig. 3). We end up with a resulting value of +3.7% for the blueshift in the PM state of $LaFe_{11.4}Si_{1.4}H_{1.6}$ at 360 K, as Fig. S10 demonstrates. This value is of the same order of magnitude as that in the FM phase. Summarizing, hydrogenation induces an overall blueshift of the Fe VDOS (phonon hardening) relative to the nonhydrogenated material. This observation agrees with the larger Fe-specific Debye temperature, Θ^{Fe}, of the hydrogenated compound (see Sec. III B and Table I) and indicates lattice hardening induced by H atoms.

B. Thermodynamic properties from NRIXS

In order to investigate the thermodynamic behavior of $LaFe_{11.4}Si_{1.6}H_{1.6}$, we extracted the (partial) Fe contribution S_{lat} to the (total) isothermal entropy S_{iso}. The contribution S_{lat} can be directly calculated from the VDOS, $g(E)$, by using the known thermodynamic relation [37,76]

$$S_{lat} = 3k_B \int_0^\infty [x \coth x - \ln(2 \sinh x)]g(E)dE, \quad (3)$$

with $x = \frac{E}{2k_BT}$. Figure 5 provides the vibrational (lattice) entropy S_{lat} per Fe atom of hydrogenated $LaFe_{11.4}Si_{1.6}H_{1.6}$ for various measurement temperatures across the metamagnetic phase transition, measured with increasing temperatures. The blue line depicts the calculated $S_{lat}(T)$ for the ferromagnetic phase from Eq. (3), calculated using the experimental VDOS at 300 K, and the red line shows the same for the paramagnetic phase, calculated from Eq. (3), using the experimentally determined $g(E)$ at 360 K. The temperature points (300 K and 360 K) have been chosen in order to be in a well-defined FM and PM state, yet being as close to the transition temperature as possible, and avoiding the possibility of beginning phase coexistence and a mixture of the two magnetic phases. There is no significant difference between data taken at zero external field and data taken at $\mu_0 H = 1.1$ T as the shift in transition temperature is only $\sim$3.5 $\frac{K}{T}$ and the transition is slightly broadened (see the Supplemental Material [49]). It can be clearly seen that both samples exhibit an offset in the entropy
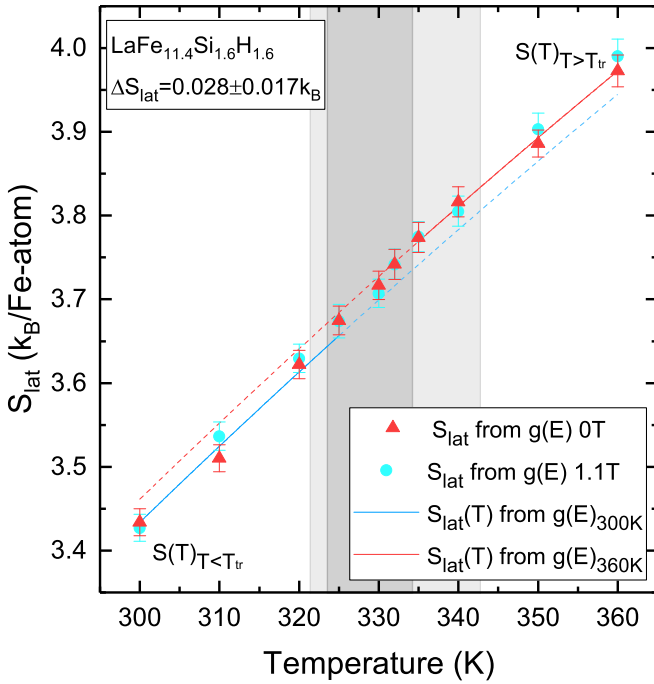
FIG. 5. Vibrational (lattice) entropy S_{lat}, calculated via Eq. (3) from the Fe-partial experimental VDOS, $g(E)$ (sample B), at several temperature points across the phase transition. $LaFe_{11.4}Si_{1.6}H_{1.6}$ exhibits an increase in S_{lat} at the FM-to-PM transition by $\Delta S_{lat} = (0.028 \pm 0.017)$ k_B/Fe atom. The blue line depicts the calculated $S_{lat}(T)$ for the ferromagnetic phase and the red line for the paramagnetic phase, calculated from Eq. (3) using the experimentally determined $g(E)$ at the given measurement temperatures, and fitted to the given entropy points in the FM region and PM region, respectively. The data points were taken with rising temperature. Red triangles: From $g(E)$ in zero external field; blue circles: from $g(E)$ in $\mu_0 H = 1.1$ T. The dark and light gray shaded areas correspond to the phase coexistence region for zero field and 1.1 T, respectively (compare with Fig. S1 of the Supplemental Material [49]). The values for S_{lat} have been extracted from VDOS (depicted in Fig. 4), which have been corrected for a residual α-Fe content of 4.47% following the method as described in [39,42].

S_{lat} after undergoing the phase transition (the hysteretic region obtained by magnetometry is indicated by the gray shaded area and vertical lines). Upon heating, the increase in the vibrational entropy (related to the redshift of the VDOS at T_{tr}) in Fig. 5 for the hydrogenated sample has a value ΔS_{lat} of (0.028 ± 0.017) k_B/Fe atom. This corresponds to $\Delta S_{lat} = 3.2 \pm 1.9 \frac{J}{kg\,K}$. The ΔS_{lat} value for the nonhydrogenated reference sample $LaFe_{11.6}Si_{1.4}$ from previous results is (0.060 ± 0.023) k_B/Fe atom, or $(6.9 \pm 2.6) \frac{J}{kg\,K}$ [42]. The increase in lattice entropy occurs in the metamagnetic phase transition region of 325–335 K ($T_{tr} = 329$ K), where the isostructural phase transition occurs, as derived from our magnetometry measurements. The change in lattice entropy ΔS_{lat} of the Fe subsystem for hydrogenated samples is found to be reduced approximately by half in comparison to nonhydrogenated compounds.

From field- and temperature-dependent magnetization measurements, we evaluated a value of $|\Delta S_{iso}| = (9.1 \pm 0.1) \frac{J}{kg\,K}$ for the isothermal entropy change from 0–1.1 T,

corresponding to the applied field used in the NRIXS measurements (see Fig. S3 of the Supplemental Material [49]). The obtained entropy change, ΔS_{lat}, of (0.028 ± 0.017) k_B/Fe atom or $(3.2 \pm 1.9) \frac{J}{kg\,K}$ for only the vibrational contribution of the Fe sublattices makes up ~35% of the total isothermal entropy change and, therefore, strongly contributes to the total entropy.

Furthermore, the entropy Debye temperatures Θ_D of the system have been calculated from the logarithmic moment of $g(E)$ [39,76–78]:

$$k_B \Theta_D = \varepsilon \exp\left[\frac{1}{3} + \int_0^\infty \ln(E/\varepsilon)\, g(E)\, dE\right]. \quad (4)$$

Here, ε is an arbitrary constant carrying the unit of energy.

The entropy Debye temperatures associated with the Fe subsystem decrease across the phase transition from the FM to the PM state by roughly 3%. We find a value for the entropy Debye temperature for the hydrogenated compound of $\Theta_{14\,K}^{Fe} = (386 \pm 7)$ K for the FM phase and a value of $\Theta_{360\,K}^{Fe} = (373 \pm 1)$ K in the PM phase (see Table I). These values are ~15 K higher than in a nonhydrogenated compound with a nominal stoichiometry of $LaFe_{11.6}Si_{1.4}$ [39]. This increase of Θ^{Fe} of approximately 4% upon hydrogenation is in agreement with the trend in the total Debye temperature Θ^{tot} obtained from measurements of the low-temperature specific heat [79]. Consistent data are also obtained from our first-principles calculations (see Table I). The agreement in Θ^{Fe} between experiment and theory is excellent.

C. Debye velocity of sound from NRIXS

The vibrational density of states (VDOS) obtained experimentally from the NRIXS data allows us to determine on the atomic level the average Debye velocity of sound, $\langle v_D \rangle$, in $LaFe_{11.4}Si_{1.6}H_{1.6}$ across the magnetostructural phase transition. $\langle v_D \rangle$ has been determined by Herlitschke *et al.* [80] employing NRIXS on the magnetocaloric material $MnFe_4Si_3$, and by Bessas *et al.* [48] on magnetocaloric $(Mn, Fe)_{1.95}(P, Si)$. The velocity of sound is an important physical quantity, which, to the best of our knowledge, surprisingly has not been considered yet in the literature for the important magnetocaloric $La(Fe, Si)_{13}$ and $La(Fe, Si)_{13}$-H compounds. The velocity of sound is a relevant quantity, e.g., for the description of ultrasonic triggering of the giant magnetocaloric effect in thin films [81]. Using the VDOS at low energies, $g(E)$, it is possible to calculate the average Debye velocity of sound, $\langle v_D \rangle$, from the following equation [82,83]:

$$\lim_{E \to 0}\left(\frac{g(E)}{E^2}\right) = \frac{m_{Fe}}{2\pi^2\, \rho\, \langle v_D \rangle^3\, \hbar^3}. \quad (5)$$

The mass of the Fe atom is $m_{Fe} = 57 \times 1.66 \times 10^{-27}$ kg. The term $\hbar$ is the reduced Planck constant. $g(E)$, at low phonon energies E, is quadratic in E. The reduced phonon DOS $\frac{g(E)}{E^2}$ can thus be described at low energies by a constant called the Debye level [48], which can be determined straightforwardly from the experimental VDOS $g(E)$ [48,80] in the limit $E \to 0$. The term ρ in Eq. (5) is the mass density of $LaFe_{11.4}Si_{1.6}H_{1.6}$, which has not yet been reported across the transition in the literature, to the best of our knowledge.
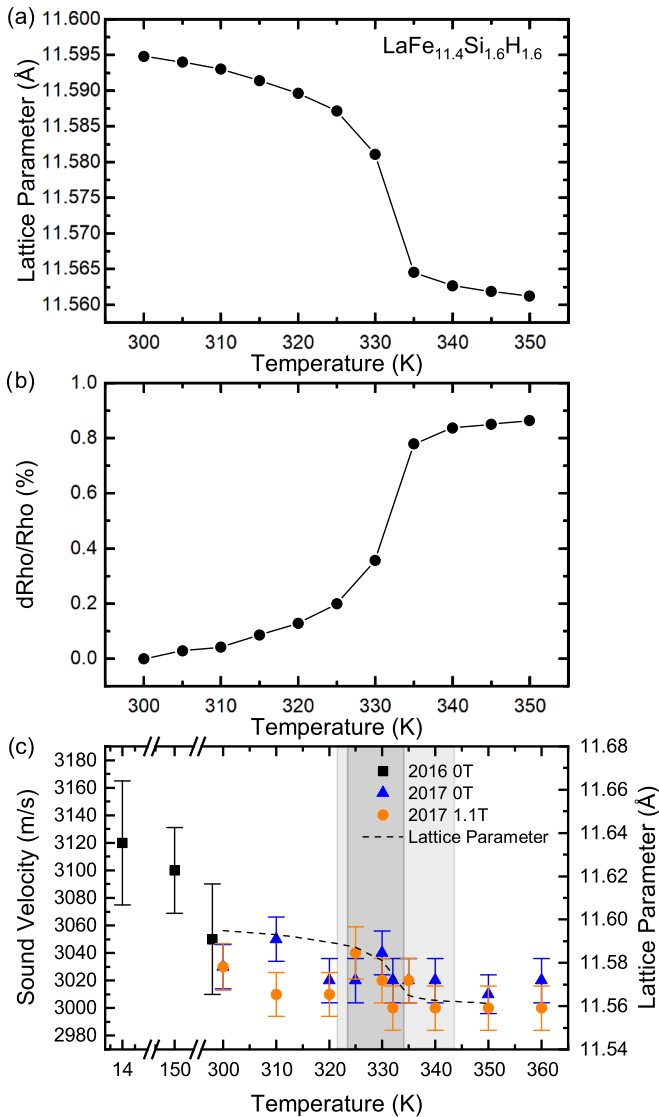
FIG. 6. Temperature dependence of the XRD lattice parameter (a), and the relative change of the mass density ρ (b) obtained from (a), for the magnetocaloric hydrogen-containing LaFe$_{11.4}$Si$_{1.6}$H$_{1.6}$ compound of natural isotopic composition (sample C) ($\rho = 6.992 \frac{g}{cm^3}$ at 300 K). (c) Temperature dependence of the mean sound velocity $\langle v_D \rangle$ (data points) compared to the change in the lattice parameter (dashed line).

Therefore, we have performed temperature-dependent PXRD measurements in the range from 300 K to 350 K on an independently prepared hydrogen-containing LaFe$_{11.4}$Si$_{1.6}$H$_{1.6}$ powder sample with natural isotopic composition (sample C, with $T_{tr} \sim 332$ K; see Sec. II). These PXRD measurements (shown in Fig. S5 of the Supplemental Material [49]) provided the lattice parameter [see Fig. 6(a)] and, consequently, the mass density ρ [see Fig. 6(b)] versus temperature across the magnetostructural transition. The drop in the lattice parameter observed in Fig. 6(a) at the first-order phase transition from the FM to the PM phase amounts to 0.29%, which is in good agreement with the change observed by neutron diffraction on deuterium-containing LaFe$_{11.44}$Si$_{1.56}$D$_{1.5}$ [25]. It can be seen in Fig. 6(b) that the mass density increases by 0.86% when

raising the temperature from 300 K (below the transition) to 350 K (above the transition).

The Debye level has been determined from $g(E)$ in the quadratic low-energy range of 5.5 meV $\leqslant E \leqslant$ 10.5 meV ($g(E)$ at energies smaller than ~ 5.0 meV are physically meaningless because of the uncertainty caused by subtraction of the central elastic (Mössbauer) peak from the NRIXS spectra; see Fig. S7 of the Supplemental Material [49]). The parabolic fit to the $g(E)$ data at low phonon energies below ~ 10.5 meV is exemplarily shown for LaFe$_{11.4}$Si$_{1.6}$H$_{1.6}$ at the lowest ($T = 14$ K) and the highest ($T = 360$ K) measurement temperature in Fig. S9 of the Supplemental Material [49]. This procedure provides a reasonable estimate of the average Debye velocity of sound for our ^{57}Fe-enriched powder sample (samples A and B). Figure 6(c) displays the average Debye velocity of sound, calculated from Eq. (5), and its temperature dependence across the phase transition. Due to the large error margins only trends in the T dependence of $\langle v_D \rangle$ can be observed in Fig. 6(c). Above the phase transition at $T_{tr} \sim 330$ K, $\langle v_D \rangle$ appears to be constant at a value of $(3020 \pm 16)\frac{m}{s}$ in zero external field (triangular blue symbols), while $\langle v_D \rangle$ in a field of 1.1 T appears to be slightly lower at $(3000 \pm 16)\frac{m}{s}$ (orange full circles). In the range between 300–350 K, the data points for $\langle v_D \rangle$ seem to follow the steplike behavior of the lattice parameter (dashed line). Below T_{tr}, $\langle v_D \rangle$ shows a trend to increase upon cooling both in zero field and applied field, and reaches a zero-field value of $(3120 \pm 45)\frac{m}{s}$ at 14 K, which is equal to an increase by $\sim 3\%$ relative to the room-temperature value of about $(3030 \pm 16)\frac{m}{s}$. The observed overall blueshift of the VDOS upon cooling (Fig. 2, bottom panel) might contribute to this effect. An increase of $\langle v_D \rangle$ upon cooling to low temperature has been observed also for magnetocaloric MnFe$_4$Si$_3$ [80]. We would like to mention that the velocity of sound determined by NRIXS [as shown in Fig. 6(c)] is connected to the THz frequency range of phonons, while ultrasound techniques probe the velocity of sound in the MHz region [80]. It was shown in Ref. [80] that the sound velocity of MnFe$_4$Si$_3$ is larger (by $\sim 7\%$ at room temperature) in the MHz regime than in the THz region. Our values for the sound velocity obtained by NRIXS [Fig. 6(c)] are somewhat smaller than those reported in Ref. [48] for magnetocaloric (MnFe)$_{1.95}$(P, Si) (FM: 3661 $\frac{m}{s}$; PM: 3267 $\frac{m}{s}$).

D. DFT calculations

The Fe partial VDOS obtained for the FM and PM states from first-principle computations agree well with the experimental VDOS measured at low temperatures ($T = 14$ K) and at $T = 360$ K $> T_C$, as demonstrated in Fig. 7. This includes Debye temperatures and the average sound velocities $\langle v_D^{Fe} \rangle$ listed in Table I. The latter were obtained from the average of $g(E)/E^2$ between 2 and 10 meV. The DFT values underestimate the experiment consistently by approximately 80 m/s, which is on the order of the error bars. We consider this an excellent confirmation, as their determination solely involves quantities determined from first-principles calculations for the slightly different composition LaFe$_{11.5}$Si$_{1.5}$H$_{1.5}$. More importantly, the difference from the sound velocities obtained from the total $g(E)$, involving the contribution from the phonon modes from all elements, is of the same
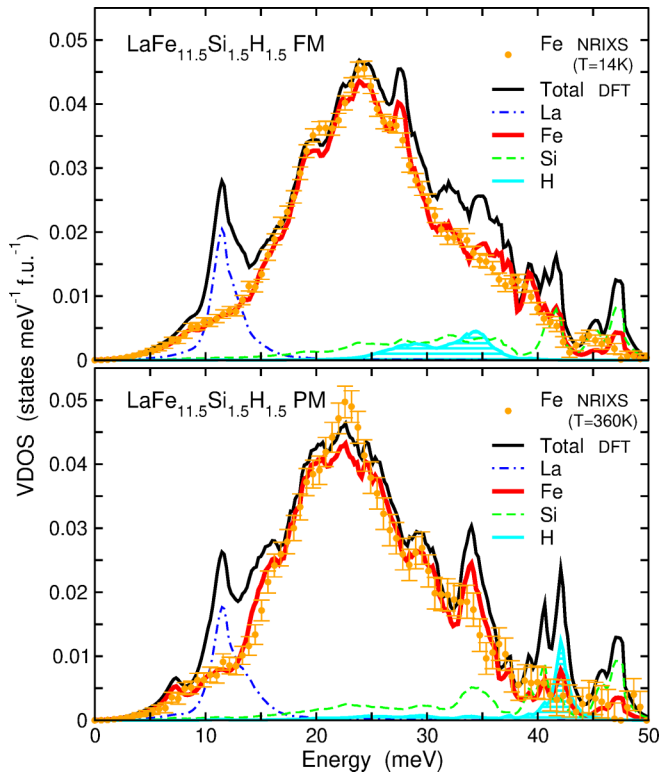
FIG. 7. DFT-calculated element-resolved VDOS of hydrogenated $LaFe_{11.5}Si_{1.5}H_{1.5}$ in the FM (top) and PM phase (bottom). Solid black lines denote the total VDOS, colored lines the element-resolved contributions: Thick red lines for Fe, dash-dotted blue lines for La, dashed green lines for Si, and solid cyan lines (with hatched area) for H. Orange circles with error bars depict the Fe-partial VDOS obtained by NRIXS at $T = 14$ K (FM) and $T = 360$ K (PM). This agrees well with the respective Fe contribution from DFT, in particular with respect to the changes in the central features discussed in the text. Note that the energy range does not cover the high-lying H modes located around 150 meV.

magnitude. This proves that the determination of the average sound velocity from element-selective NRIXS measurements of the Fe-partial $g(E)$ provides an accurate estimate of this quantity.

DFT predicts a redshift in first moment in $\langle E^1 \rangle$ of the $g(E)$ of -5.4% from the FM to the PM phase (see Table I), which is similar to the experimental value of -3.1%. This trend is similar to the nonhydrogenated case, where we find $\langle E^1 \rangle = 25.41$ meV for the FM and 23.00 meV for the PM, resulting in a significant redshift of -9.4%, qualitatively consistent with the experimental value of -3.7% in the range from 62 K to 301 K. Comparing the changes in $\langle E^1 \rangle$ upon hydrogenation within the FM and PM structures, we obtain in both cases a blueshift of $+0.7\%$ and $+5.3\%$, respectively, which again reflects the experimental trend ($+2.1\%$ and $+3.7\%$ for the FM and PM phase, respectively; see Fig. S10 of the Supplemental Material [49]). This proves that the hardening of the Fe sublattice through hydrogenation is indeed an intrinsic effect, originating from the incorporation of H on the interstitial 24d sites.

Even fine details of the experimental VDOS are represented in the calculated VDOS. Apart from the broadening of

the peaks around the central maximum at 18 and 28 meV, this includes in particular the average redshift of the entire DOS and the disappearance of the broadened 28 meV feature in the PM phase. For the hydrogen-free case, this was interpreted as an indication of the strong magnetoelastic coupling present in the system [39,42]. One-third of the hydrogen vibrational modes are found at comparatively low energies. This stands in contrast to the general expectation for light elements, which are supposed to mark the high-frequency end of the vibrational spectrum. In the present case, the lowest hydrogen modes occupy the same energy range as the 28-times heavier Si atoms, i.e., between 15 and 50 meV. According to the low mass, we must expect the exact shape and position of the H VDOS obtained from our calculations to be particularly sensitive to the technical settings, including the modeling of magnetic disorder. Nevertheless, the low energy of some H modes indicates a very shallow direction on the binding surface, where the H atoms can move almost freely. In other directions this is not the case, since the other two-thirds of the vibrational states are distributed between two sharp peaks centered around 150 meV (omitted in Fig. 7). For equiatomic LaFeSiH (tetragonal $P4/nmm$ symmetry) it was recently reported that the vast majority of H modes is seen above 100 meV, but again a fraction of H modes was found at low energies around 10 meV [84].

The element-resolved electronic DOS (Fig. 8) is in close agreement with the DFT calculation of Gercsi *et al.* [43], which uses a slightly different setup, where Si replaces Fe on the Fe_I 8b sites instead of the Fe_{II} 96i sites. Figure 8 reveals a hybridization of the H and Fe states at around -7.5 eV, which is below the d-band edge of Fe in the hydrogen-free compound. Such a feature is necessary to explain the stability of the hydrogenated La-Fe-Si, which corresponds to a gain in formation energy due to the hydrogen uptake. In turn, there is only a negligible density of states with H character at the Fermi level, which is thus dominated by the d states of Fe in the FM and in the PM phase. Comparing both phases, we see a picture that is completely analogous to the hydrogen-free compound. The DOS of the FM phase is characterized by a pronounced minimum in the minority spin channel right at E_{Fermi} (cf. the arrow in the upper panel of Fig. 8), which is responsible for stabilizing the comparatively high magnetic moment of 24.4 μ_B/f.u. (or 2.2 μ_B/Fe, respectively), which is likewise characteristic for the hydrogen-free compound.

Modeling the PM state of $LaFe_{11.5}Si_{1.5}H_{1.5}$ in the same way as reported in [39,61] for $LaFe_{11.5}Si_{1.5}$ leads once again to very similar characteristic changes in the DOS, as shown in the lower panel of Fig. 8: The enforced hybridization of minority and majority d states of Fe atoms with reversed magnetic orientation leads to the broadening of the features, including the minimum at E_{Fermi} in combination with a reduction of the local magnetic moment of Fe to 1.8 μ_B/Fe. The result is a decreased exchange splitting, moving the smeared-out minority spin minimum to 0.5–1 eV below E_{Fermi}, as indicated by the arrows in the lower panel of Fig. 8. The important consequence is again a significantly increased DOS at E_{Fermi} in the PM phase, which gives rise to the anomalous softening of the vibrational modes in the PM phase due to adiabatic electron-phonon coupling [39,85–88]. These observations are consistent with earlier temperature-dependent
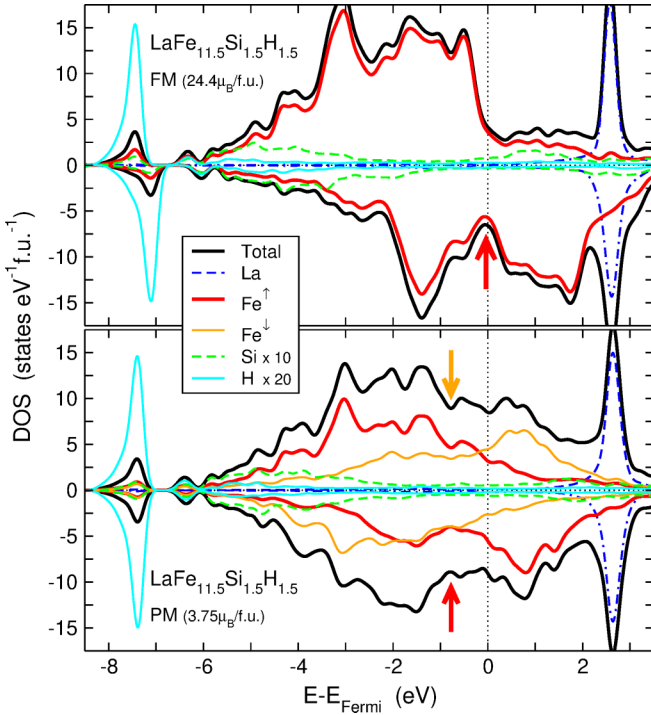
FIG. 8. Spin-resolved element- and site-resolved electronic density of states $D(E)$ of hydrogenated $LaFe_{11.5}Si_{1.5}H_{1.5}$ in the FM (top panel) and PM (bottom panel) phase obtained from DFT. Black lines indicate the total DOS of each spin channel, while blue (dash-dotted) and red (solid) lines denote the partial DOS of La and $Fe^{\uparrow}$. In the PM state, part of the Fe atoms have opposite magnetic orientation ($Fe^{\downarrow}$). Their contribution is indicated by the orange lines. For better visibility, their partial contributions of Si (green dashed lines) and H (cyan solid lines) are enlarged by a factor of 10 and 20, respectively. The deep minority spin minimum at the Fermi energy E_{Fermi} for the FM state is depicted by the vertical red arrow. The red and orange arrows in the bottom panel indicate the shift of the minimum in the minority channel of the respective site-projected Fe DOS ($Fe^{\uparrow}$ and $Fe^{\downarrow}$).

measurements of the thermopower [89], which is sensitive to the features in the electronic DOS close to the Fermi energy. One finds, despite some differences in the absolute numbers, a rather similar shape of its characteristic change across the phase transition for the hydrogenated and nonhydrogenated compounds.

In analogy to the hydrogen-free case [39], we can substantiate this picture by comparing the site-resolved minority spin density of states and the computed entropy change at the phase transition, as shown in Fig. 9. The thin lines in the left panel show the entropy change as a function of temperature calculated according to Eq. (3) from the respective site-resolved VDOS in the FM and PM state in Fig. 7. The thick lines correspond to the elemental averages. From Fig. 9 (left) we can directly see that only the Fe sites contribute to the cooperative entropy change at the FM-PM transition. The contribution of Si is negligible, whereas La and H exhibit a decrease in entropy, as expected according to the smaller volume in the PM phase. Their absolute contribution per site is, however, much smaller in comparison to Fe. Thus, the presence of H affects neither ΔS_{lat} nor ΔS_{el} at T_{tr} significantly.
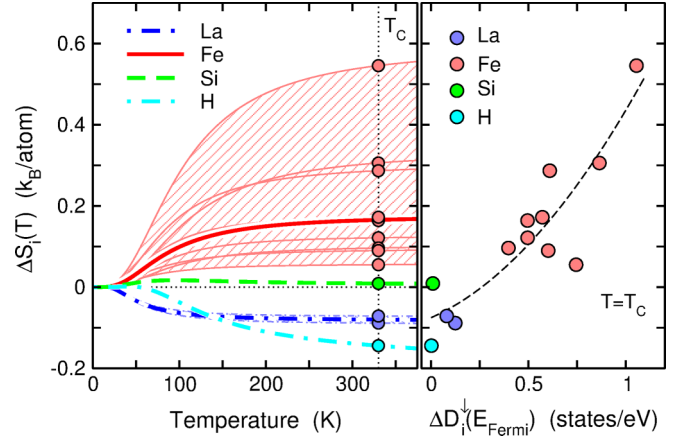

FIG. 9. Entropy difference $\Delta S_i = S_i(PM) - S_i(FM)$ associated with lattice site i as a function of temperature (left panel) calculated from the element- and site-resolved FM and PM VDOS obtained by DFT. The thick lines denote the element-specific averages. In the right panel, the site-resolved entropy change (circles) at $T_{tr} = 329\,K$ is plotted against the change in the site-projected minority spin density of states at the Fermi level $\Delta D_i^{\downarrow}(E_{Fermi})$. The dashed line illustrates as a guide to the eye the correlation between the two quantities. We interpret this as a consequence of the adiabatic electron-phonon coupling in hydrogenated La-Fe-Si.

We ascribe this to the low density of H states in the energy range above -6 eV, where they could hybridize with the Fe-d states, which are particularly sensitive to the change in magnetic order.

In absolute numbers, the DFT calculations predict an entropy change ΔS_{lat} related to the Fe sites at T_{tr} of 0.16 k_B/Fe, which is, in analogy to the magnitude of the redshift in $\langle E^1 \rangle$, significantly larger compared to the experimental value of (0.028 ± 0.017) k_B/Fe atom reported above. We ascribe this to the fact that we use idealized models of both phases in the calculations, while the experimental values were obtained in close proximity to the phase transition. Thus, in the calculations, we miss the finite-temperature excitations of the magnetic subsystem and the associated (negative) thermal expansion in the FM phase. In turn, in the PM phase, residual FM order (or FM short-range order) may still be present in the PM phase close to T_{tr}. A likewise overestimation of the entropy change has also been discussed for the nonhydrogenated compound [39,42]. If we thus compare the relative changes upon hydrogenation, we find a reduction in ΔS_{lat} of about 50% after adding hydrogen, consistently in theory and experiment. This is in agreement with the thermodynamic analysis of Gercsi et al. [43], who concluded on a decrease of electron-phonon coupling after hydrogenation.

The site-resolved entropy corresponds to the phase space occupied by the relevant degrees of freedom of a specific ion. Thus, vibrational entropy can be seen as measure of the elastic properties of the lattice, since a vibrating ion can occupy more phase space if it moves in a softer potential. The mechanism of adiabatic electron-phonon coupling links the availability of states at the Fermi level to the vibrational properties of the system [85–88]. This has been identified as the source of the anomalous softening in the hydrogen-free

system [39,42,61]. Accordingly, we expect that also in the hydrogenated compound the disappearance of the minority spin minimum at E_{Fermi} should lead to a softening of the lattice, which is consequently reflected in a larger entropy at a given temperature. The right panel of Fig. 9 proves that such a correlation indeed exists, if we compare for each inequivalent lattice site i the entropy change at T_{tr} with the change in the local, site-resolved minority spin density of states, taken at the Fermi level.

IV. CONCLUSION

We precisely determined the Fe-partial vibrational (phonon) density of states (VDOS) for hydrogenated $\text{LaFe}_{11.4}\text{Si}_{1.6}\text{H}_{1.6}$ by means of ^{57}Fe NRIXS measurements. We observed characteristic differences in the shape of the VDOS for hydrogenated compounds in comparison to the nonhydrogenated ones, which are confirmed by first-principles calculations of the element-resolved VDOS in the framework of density functional theory (DFT). The temperature evolution of the VDOS across the isostructural phase transition for hydrogenated $\text{LaFe}_{11.4}\text{Si}_{1.6}\text{H}_{1.6}$ shows a similar overall trend to that observed in nonhydrogenated compounds, but the details are very different. An overall energetic redshift of the VDOS near T_{tr} upon heating can be seen despite the volume decrease, when undergoing the isostructural first-order phase transition. Moreover, a striking overall blueshift upon hydrogenation is revealed in the Fe VDOS for the FM as well as for the PM state (phonon hardening), which is in line with the enhanced Fe-specific Debye temperature observed. Furthermore, from the low-energy part of the experimental Fe-partial VDOS, we determined the average Debye velocity of sound of $\text{LaFe}_{11.4}\text{Si}_{1.6}\text{H}_{1.6}$ and its temperature dependence. $\langle v_D \rangle$ is found to be enhanced by $\sim 3\%$ in the low-T FM state relative to the high-T PM state.

Our DFT calculations show that similarly to the hydrogen-free compound, this anomalous behavior must be attributed to adiabatic electron phonon coupling, which causes the overall lattice softening in the compound at the FM-to-PM transition. It is traced back to the change in the site-resolved minority spin density of states, originating from a characteristic minimum in the minority spin density of states of the FM right at the Fermi level, which shifts and broadens in the magnetically disordered state. From these results and the reduction of the entropy jump upon heating by 50% due to hydrogenation, we conclude on a reduction of the adiabatic electron-phonon coupling, confirming the previous conjecture of Gercsi *et al.* [43] based on different experimental and theoretical data.

In addition, we observe a strong reduction of prominent phonon modes and a broadening of the phonon peaks upon hydrogenation. The Fe-specific phonon mode at $\sim 27\,\text{meV}$ is reduced to a shoulder in the hydrogenated compound, which disappears after undergoing the phase transition from the FM to the PM state. Interestingly, the phonon mode near 18 meV, which is retained in the PM state of nonhydrogenated $\text{LaFe}_{11.6}\text{Si}_{1.4}$, is strongly quenched in the PM state due to hydrogenation. These effects are another microscopic manifestation of strong magnetoelastic coupling in $\text{LaFe}_{11.4}\text{Si}_{1.6}\text{H}_{1.6}$. Our results reveal that hydrogen not only shifts the

temperature of the first-order transition but also significantly affects the magnetoelastic response of the Fe subsystem, as observed experimentally and theoretically. We would like to mention that NRIXS investigations on other magnetocaloric materials [48,80], although they also demonstrated a clear redshift in the Fe-partial VDOS across the first-order phase transition, did not reveal any changes in the shape of the Fe-partial VDOS across the transition. Thus, $\text{La}(\text{Fe, Si})_{13}$ and $\text{La}(\text{Fe, Si})_{13}\text{H}$ appear to be exceptional materials with respect to strong adiabatic electron phonon interaction and strong spin phonon coupling for particular Fe-specific phonon modes. The fingerprint of pronounced spin-phonon coupling is the Fe-specific phonon mode near 27 meV in both nonhydrogenated and hydrogenated $\text{La}(\text{Fe, Si})_{13}$.

In this context it is interesting that a remarkable phonon peak at the same energy ($\sim 28\,\text{meV}$) (also related to Fe vibrations) has been predicted for superconducting LaFeSiH (the 1:1:1:1 compound) [84]. This suggests that this Fe phonon mode has the same origin in these materials and experiences strong electron-phonon interaction. Future ^{57}Fe NRIXS experiments are needed to support this assumption.

From the VDOS we derived the vibrational (lattice) entropy S_{lat} of the Fe subsystem across the magnetostructural phase transition. For $\text{LaFe}_{11.4}\text{Si}_{1.6}\text{H}_{1.6}$ the vibrational entropy S_{lat}, directly extracted from the Fe partial VDOS, $g(E)$, exhibits an increase by $(0.028 \pm 0.017)\,k_B/\text{Fe atom [or}$ $(3.2 \pm 1.9)\,\frac{\text{J}}{\text{kg K}}]$ upon heating across the transition temperature ($T_{\text{tr}} = 329\,\text{K}$). This value is found to be only half the value of nonhydrogenated compounds [42], which agrees well with the trend of the values found by first-principles calculations. It contributes with $\sim 35\%$ to the overall isothermal entropy change ΔS_{iso} at T_{tr} [$(9.1 \pm 0.1)\,\frac{\text{J}}{\text{kg K}}$]. Accordingly, the entropy Debye temperature of the Fe subsystem Θ_D^{Fe}, which turns out to be approximately 4% larger than in the hydrogen-free case, exhibits a decrease of $\sim 3\%$ from the FM to the PM state.

Although we have observed distinct modifications in the vibrational density of states (VDOS) and electronic DOS and a 50% reduction in ΔS_{lat} in hydrogenated $\text{La}(\text{Fe, Si})_{13}\text{H}$ as compared to the nonhydrogenated material, the total change ΔS_{iso} is known to be almost the same for the two materials at their respective transition temperatures [31]. Thus, the $\sim 50\%$ decrease of ΔS_{lat} in the hydrogenated material must be compensated by other terms in Eq. (1) above.

Regarding the fact that a hydrogen atom provides an extra electron to the conduction electron density of states, we can look for other elements with such a property. Recently, a huge entropy change of $\Delta S_{\text{mag}} = 31.4\,\frac{\text{J}}{\text{kg K}}$ at a magnetic field change of only 3 T was reported [90] for the slightly P-doped $\text{LaFe}_{11.6}\text{Si}_{1.4}\text{P}_{0.03}$ compound near the Curie temperature of 194 K, with the P atoms most likely occupying 96i sites, like Fe and Si atoms. As P atoms have an outer shell of $3s^2 3p^3$, P adds one electron more than a Si atom ($2s^2 2p^2$) to the conduction electron system. In order to check whether this effect contributes to this observed giant ΔS_{mag} enhancement, doping (possibly by nonequilibrium techniques, such as splat cooling, melt spinning, or ion implantation) with other elements in the IVa column of the periodic table (As, Sb, Bi) could be of interest.

Our work proves that while hydrogenation is capable of shifting the transition to ambient conditions, the inherent adiabatic electron-phonon coupling and large moment-volume coupling [61] remain effective. These are associated with the itinerant electron metamagnetism, which determines the characteristic properties of the hydrogen-free system. Thus the cooperative contribution of the various degrees of freedom to the magnetocaloric effect persists after hydrogenation, which contributes to the superior magnetocaloric performance of this system.

ACKNOWLEDGMENTS

[1] S. Fähler, U. K. Rößler, O. Kastner, J. Eckert, G. Eggeler, H. Emmerich, P. Entel, S. Müller, E. Quandt, and K. Albe, Adv. Eng. Mater. **14**, 10 (2012).

[2] X. Moya, S. Kar-Narayan, and N. D. Mathur, Nat. Mater. **13**, 439 (2014).

[3] V. K. Pecharsky and K. A. Gschneidner, Phys. Rev. Lett. **78**, 4494 (1997).

[4] K. A. Gschneidner, Jr., V. K. Pecharsky, and A. O. Tsokol, Rep. Prog. Phys. **68**, 1479 (2005).

[5] N. H. Dung, Z. Q. Ou, L. Caron, L. Zhang, D. T. C. Than, G. A. de Wijs, R. A. de Groot, K. H. J. Buschow, and E. Brück, Adv. Energy Mater. **1**, 1215 (2011).

[6] M. F. J. Boeije, P. Roy, F. Guillou, H. Yibole, X. Miao, L. Caron, D. Banerjee, N. H. van Dijk, R. A. de Groot, and E. Brück, Chem. Mater. **28**, 4901 (2016).

[7] A. Waske, M. E. Gruner, T. Gottschall, and O. Gutfleisch, MRS Bull. **43**, 269 (2018).

[8] A. Tishin, Y. Spichkin, V. Zverev, and P. Egolf, Int. J. Refrigeration **68**, 177 (2016).

[9] O. Gutfleisch, T. Gottschall, M. Fries, D. Benke, I. Radulov, K. P. Skokov, H. Wende, M. Gruner, M. Acet, P. Entel, and M. Farle, Philos. Trans. R. Soc., A **374**, 20150308 (2016).

[10] K. G. Sandeman, Scr. Mater. **67**, 566 (2012).

[11] J. Lyubina, R. Schäfer, N. Martin, L. Schultz, and O. Gutfleisch, Adv. Mater. **22**, 3735 (2010).

[12] S. Fujieda, A. Fujita, and K. Fukamichi, Appl. Phys. Lett. **81**, 1276 (2002).

[13] S. Fujieda, A. Fujita, K. Fukamichi, Y. Yamazaki, and Y. Iijima, Appl. Phys. Lett. **79**, 653 (2001).

[14] J. Liu, M. Krautz, K. Skokov, T. G. Woodcock, and O. Gutfleisch, Acta Mater. **59**, 3602 (2011).

[15] F. Hu, M. Ilyn, A. M. Tishin, J. R. Sun, G. J. Wang, Y. F. Chen, F. Wang, Z. H. Cheng, and B. G. Shen, J. Appl. Phys. **93**, 5503 (2003).

[16] F. Hu, B. Shen, J. Sun, Z. Cheng, G. Rao, and X. Zhang, Appl. Phys. Lett. **78**, 3675 (2001).

[17] M. D. Kuz'min and M. Richter, Phys. Rev. B **76**, 092401 (2007).

[18] A. Tishin and Y. Spichkin, *The Magnetocaloric Effect and Its Applications*, Condensed Matter Physics (CRC Press, Bristol, Philadelphia, 2003).

[19] O. Gutfleisch, M. A. Willard, E. Brück, C. H. Chen, S. G. Sankar, and J. P. Liu, Adv. Mater. **23**, 821 (2011).

[20] A. Fujita, Y. Akamatsu, and K. Fukamichi, J. Appl. Phys. **85**, 4756 (1999).

[21] H. Hamdeh, H. Al-Ghanem, W. Hikal, S. Taher, J. Ho, D. Anh, N. Thuy, N. Duc, and P. Thang, J. Magn. Magn. Mater. **269**, 404 (2004).

[22] M. Rosca, M. Balli, D. Fruchart, D. Gignoux, E. Hlil, S. Miraglia, B. Ouladdiaf, and P. Wolfers, J. Alloys Compd. **490**, 50 (2010).

[23] L. Jia, G. J. Liu, J. R. Sun, H. W. Zhang, F. X. Hu, C. Dong, G. H. Rao, and B. G. Shen, J. Appl. Phys. **100**, 123904 (2006).

[24] J. Y. Law, V. Franco, L. M. Moreno-Ramírez, A. Conde, D. Y. Karpenkov, I. Radulov, K. P. Skokov, and O. Gutfleisch, Nat. Commun. **9**, 2680 (2018).

[25] S. Fujieda, A. Fujita, K. Fukamichi, Y. Yamaguchi, and K. Ohoyama, J. Phys. Soc. Jpn. **77**, 074722 (2008).

[26] M. Krautz, K. Skokov, T. Gottschall, C. S. Teixeira, A. Waske, J. Liu, L. Schultz, and O. Gutfleisch, J. Alloys Compd. **598**, 27 (2014).

[27] J. Wang, Y. Chen, Y. Tang, S. Xiao, T. Liu, and E. Zhang, J. Alloys Compd. **485**, 313 (2009).

[28] M. Phejar, V. Paul-Boncour, and L. Bessais, J. Solid State Chem. **233**, 95 (2016).

[29] X. Hai, F. Porcher, C. Mayer, and S. Miraglia, J. Appl. Phys. **123**, 085115 (2018).

[30] S. Rundqvist, R. Tellgren, and Y. Andersson, J. Less-Common Met. **101**, 145 (1984).

[31] A. Fujita, S. Fujieda, Y. Hasegawa, and K. Fukamichi, Phys. Rev. B **67**, 104416 (2003).

[32] J. Lyubina, K. Nenkov, L. Schultz, and O. Gutfleisch, Phys. Rev. Lett. **101**, 177203 (2008).

[33] M. Krautz, J. D. Moore, K. P. Skokov, J. Liu, C. S. Teixeira, R. Schäfer, L. Schultz, and O. Gutfleisch, J. Appl. Phys. **112**, 083918 (2012).

[34] A. Barcza, M. Katter, V. Zellmann, S. Russek, S. Jacobs, and C. Zimm, IEEE Trans. Magn. **47**, 3391 (2011).

[35] F. Wang, G. Wang, F. Hu, A. Kurbakov, B. Shen, and Z. Cheng, J. Phys.: Condens. Matter **15**, 5269 (2003).

[36] O. L. Baumfeld, Z. Gercsi, M. Krautz, O. Gutfleisch, and K. G. Sandeman, J. Appl. Phys. **115**, 203905 (2014).

[37] B. Fultz, Prog. Mater. Sci. **55**, 247 (2010).

[38] F. Scheibel, T. Gottschall, A. Taubel, M. Fries, K. P. Skokov, A. Terwey, W. Keune, K. Ollefs, H. Wende, M. Farle, M. Acet, O. Gutfleisch, and M. E. Gruner, Energy Technol. **6**, 1397 (2018).

[39] M. E. Gruner, W. Keune, B. Roldan Cuenya, C. Weis, J. Landers, S. I. Makarov, D. Klar, M. Y. Hu, E. E. Alp, J. Zhao, M. Krautz, O. Gutfleisch, and H. Wende, Phys. Rev. Lett. **114**, 057202 (2015).

[40] M. Piazzi, C. Bennati, C. Curcio, M. Kuepferling, and V. Basso, J. Magn. Magn. Mater. **400**, 349 (2016).

[41] V. Basso, M. Piazzi, C. Bennati, and C. Curcio, Phys. Status Solidi B **255**, 1700278 (2017).

[42] J. Landers, S. Salamon, W. Keune, M. E. Gruner, M. Krautz, J. Zhao, M. Y. Hu, T. S. Toellner, E. E. Alp, O. Gutfleisch, and H. Wende, Phys. Rev. B **98**, 024417 (2018).

[43] Z. Gercsi, N. Fuller, K. G. Sandeman, and A. Fujita, J. Phys. D: Appl. Phys. **51**, 034003 (2018).

[44] K. S. Singwi and A. Sjølander, Phys. Rev. **120**, 1093 (1960).

[45] M. Seto, Y. Yoda, S. Kikuta, X. W. Zhang, and M. Ando, Phys. Rev. Lett. **74**, 3828 (1995).

[46] W. Sturhahn, T. S. Toellner, E. E. Alp, X. Zhang, M. Ando, Y. Yoda, S. Kikuta, M. Seto, C. W. Kimball, and B. Dabrowski, Phys. Rev. Lett. **74**, 3832 (1995).

[47] A. I. Chumakov, R. Rüffer, H. Grünsteudel, H. F. Grünsteudel, G. Grübel, J. Metge, O. Leupold, and H. A. Goodwin, Europhys. Lett. **30**, 427 (1995).

[48] D. Bessas, M. Maschek, H. Yibole, J.-W. Lai, S. M. Souliou, I. Sergueev, A. I. Dugulan, N. H. van Dijk, and E. Brück, Phys. Rev. B **97**, 094303 (2018).

[49] See Supplemental Material at http://link.aps.org/supplemental/10.1103/PhysRevB.101.064415 for raw data and normalized excitation probability data.

[50] S. I. Makarov, M. Krautz, S. Salamon, K. Skokov, C. S. Teixeira, O. Gutfleisch, H. Wende, and W. Keune, J. Phys. D: Appl. Phys. **48**, 305006 (2015).

[51] T. Faske and W. Donner, J. Appl. Crystallogr. **51**, 761 (2018).

[52] J. Neuhaus, M. Leitner, K. Nicolaus, W. Petry, B. Hennion, and A. Hiess, Phys. Rev. B **89**, 184302 (2014).

[53] M. Kresch, Temperature dependence of phonons in elemental cubic metals studied by inelastic scattering of neutrons and x-rays, Ph.D. thesis, California Institute of Technology, 2009.

[54] H. Hasegawa, M. W. Finnis, and D. G. Pettifor, J. Phys. F: Met. Phys. **15**, 19 (1985).

[55] R. Boehler and J. Ramakrishnan, J. Geophys. Res. **85**, 6996 (1980).

[56] A. Chumakov and W. Sturhahn, Hyperfine Interact. **123–124**, 781 (1999).

[57] W. Sturhahn and V. Kohn, Hyperfine Interact. **123–124**, 367 (1999).

[58] T. Toellner, Hyperfine Interact. **125**, 3 (2000).

[59] W. Sturhahn, J. Phys.: Condens. Matter **16**, S497 (2004).

[60] U. von Hörsten, Pi Program Package, http://www.uni-due.de/~hm236ap/hoersten/home.html.

[61] M. E. Gruner, W. Keune, J. Landers, S. Salamon, M. Krautz, J. Zhao, M. Y. Hu, T. Toellner, E. E. Alp, O. Gutfleisch, and H. Wende, Phys. Status Solidi B **255**, 1700465 (2018).

[62] G. Kresse and J. Furthmüller, Phys. Rev. B **54**, 11169 (1996).

[63] G. Kresse and D. Joubert, Phys. Rev. B **59**, 1758 (1999).

[64] J. P. Perdew, in *Electronic Structure of Solids '91*, edited by P. Ziesche and H. Eschrig (Akademie Verlag, Berlin, 1991).

[65] J. P. Perdew, K. Burke, and Y. Wang, Phys. Rev. B **54**, 16533 (1996).

[66] S. H. Vosko, L. Wilk, and M. Nusair, Can. J. Phys. **58**, 1200 (1980).

[67] G. Kresse, J. Furthmüller, and J. Hafner, Europhys. Lett. **32**, 729 (1995).

[68] X. Gonze and C. Lee, Phys. Rev. B **55**, 10355 (1997).

[69] K. Parlinski, Z. Q. Li, and Y. Kawazoe, Phys. Rev. Lett. **78**, 4063 (1997).

[70] D. Alfè, Comput. Phys. Commun. **180**, 2622 (2009).

[71] A. R. Williams, V. L. Moruzzi, J. Kübler, and K. Schwarz, Bull. Am. Phys. Soc. **29**, 278 (1984).

[72] K. Schwarz and P. Mohn, J. Phys. F: Met. Phys. **14**, L129 (1984).

[73] P. H. Dederichs, S. Blügel, R. Zeller, and H. Akai, Phys. Rev. Lett. **53**, 2512 (1984).

[74] V. L. Moruzzi, P. M. Marcus, K. Schwarz, and P. Mohn, Phys. Rev. B **34**, 1784 (1986).

[75] C. Kittel, *Introduction to Solid State Physics*, 5th ed. (John Wiley & Sons, New York, 1976), p. 152.

[76] G. Grimvall, *Thermophysical Properties of Materials*, Selected Topics in Solid State Physics Vol. 18 (North-Holland, Amsterdam, 1986).

[77] J. Rosén and G. Grimvall, Phys. Rev. B **27**, 7199 (1983).

[78] O. Eriksson, J. M. Wills, and D. Wallace, Phys. Rev. B **46**, 5221 (1992).

[79] E. Lovell, L. Ghivelder, A. Nicotina, J. Turcaud, M. Bratko, A. D. Caplin, V. Basso, A. Barcza, M. Katter, and L. F. Cohen, Phys. Rev. B **94**, 134405 (2016).

[80] M. Herlitschke, B. Klobes, I. Sergueev, P. Hering, J. Perßon, and R. P. Hermann, Phys. Rev. B **93**, 094304 (2016).

[81] J.-Y. Duquesne, J.-Y. Prieur, J. A. Canalejo, V. H. Etgens, M. Eddrief, A. L. Ferreira, and M. Marangolo, Phys. Rev. B **86**, 035207 (2012).

[82] K. Achterhold, C. Keppler, A. Ostermann, U. van Bürck, W. Sturhahn, E. E. Alp, and F. G. Parak, Phys. Rev. E **65**, 051916 (2002).

[83] M. Y. Hu, W. Sturhahn, T. S. Toellner, P. D. Mannheim, D. E. Brown, J. Zhao, and E. E. Alp, Phys. Rev. B **67**, 094304 (2003).

[84] L. Hung and T. Yildirim, Phys. Rev. B **97**, 224501 (2018).

[85] O. Delaire, M. S. Lucas, J. A. Muñoz, M. Kresch, and B. Fultz, Phys. Rev. Lett. **101**, 105504 (2008).

[86] M. S. Lucas, J. A. Muñoz, O. Delaire, N. D. Markovskiy, M. B. Stone, D. L. Abernathy, I. Halevy, L. Mauger, J. B. Keith, M. L. Winterrose, Y. Xiao, M. Lerche, and B. Fultz, Phys. Rev. B **82**, 144306 (2010).

[87] O. Delaire, K. Marty, M. B. Stone, P. R. C. Kent, M. S. Lucas, D. L. Abernathy, D. Mandrus, and B. C. Sales, Proc. Natl. Acad. Sci. USA **108**, 4725 (2011).

[88] B. Fultz, *Phase Transitions in Materials* (Cambridge University Press, Cambridge, UK, 2014).

[89] U. Hannemann, J. Lyubina, M. P. Ryan, N. M. Alford, and L. F. Cohen, Europhys. Lett. **100**, 57009 (2012).

[90] P. Jin, Y. Li, Y. Dai, Z. Xu, C. Song, Z. Luo, Q. Zhai, K. Han, and H. Zheng, Metals **9**, 432 (2019).